Journal of the European Ceramic Society 38 (2018) 3472–3477

Contents lists available at ScienceDirect

Journal of the European Ceramic Society

journal homepage: www.elsevier.com/locate/jeurceramsoc

Original Article

In-situ TEM study of the aging micromechanisms in a $BaTiO_3$-based lead-free piezoelectric ceramic

Zhongming Fan, Xiaoli Tan*

Department of Materials Science and Engineering, Iowa State University, Ames, IA, 50011, USA

ARTICLE INFO

Keywords:
Aging
Fatigue
In-Situ
TEM
BZT–BCT
Domain disruption

ABSTRACT

Aging and fatigue are the two main concerns regarding the performance reliability of piezoelectric ceramics. Compared with fatigue, less efforts have been made towards clarifying the micromechanisms of aging. In this report, we employ electric field *in-situ* transmission electron microscopy (TEM) to directly visualize the domain structure evolution during fatigue and the subsequent aging process in the $0.5Ba(Zr_{0.2}Ti_{0.8})O_3$–$0.5(Ba_{0.7}Ca_{0.3})TiO_3$ (BZT–BCT) polycrystalline ceramic. The macroscopic aging behaviors, including the development of internal bias field (E_{bias}) and the degradation in switchable polarization ($2P_r$), are correlated with the microscopic domain wall clamping and domain disruption resulted from the redistribution of oxygen vacancies driven by depolarization field.

1. Introduction

Piezoelectric ceramics have found applications in a variety of devices including sensors, transducers, and actuators [1,2]. The primary pursuit in optimizing the piezoelectric ceramic composition is to achieve high functional properties, most importantly the piezoelectric coefficient (d_{33}). Piezoelectric properties inevitably degrade due to electric fatigue during electrical cycling or aging with time even without any applied fields [3]. Actually, real piezoelectric devices suffer from both fatigue and aging because they are subjected to cyclic fields while working and zero fields while sitting idle. It has been realized that long-term performance stability and reliability is of equal importance as high properties to practical devices. Therefore, investigations on the micromechanisms of fatigue and aging are critical to composition optimization and device design.

In fact, electric fatigue has been studied more comprehensively than aging in the literature. Various experimental methods are employed to uncover the microstructural origin of the fatigue degradation. Piezoresponse force microscopy has been extensively used to reveal the change in domain morphology before and after electrical cycling [4–6]. TEM, capable of providing chemical and crystallographic information and imaging nanoscale defects, starts to make contributions to electric fatigue research. Our previous electric field *in-situ* TEM experiments have successfully identified various microstructural mechanisms of fatigue degradation, including domain fragmentation [7], domain formation blockage [8], and microcrack initiation [9].

In contrast, the research on aging degradation has been mainly focused on interpretations of macroscopic results and analytical modelling of the experimental data [3]. Aging in piezoelectric ceramics can be generally classified into two categories, aging in the unpoled state and aging in the poled state. Aging in the unpoled state can result in the "pinching" of polarization-electric field (*P-E*) hysteresis loop, whereas aging in the poled state leads to the shift of the *P-E* loop [3]. Three major models have been proposed to explain these aging phenomena. Volume effect is associated with the symmetry-conforming defect dipoles, consisting of oxygen vacancy and acceptor cation pairs, that align themselves during aging with the spontaneous polarization in a ferroelectric domain [10]. The volume effect has succeeded in explaining the recoverable electro-strain and the double *P-E* loops in aged unpoled ceramics [11]. Domain wall effect, where domain walls are gradually pinned by charged point defects during aging, is more extensively discussed as the cause of fatigue than of aging [12–14]. Grain boundary effect, or the space charge model, describes the accumulation of charged point defects at grain boundaries during aging, which stabilizes the existing domain configuration [15,16]. The space charge model has been rather effective in reproducing the time dependence of the internal bias field (E_{bias}) development during aging of poled ceramics [17,18].

In spite of the considerable experimental and modelling efforts, direct observation on microstructure evolution during aging has not yet been reported. In the present work, a test profile that mimics the intermittent working conditions of practical piezoelectric devices, i.e., aging after cyclic electrical loadings, is applied to BZT–BCT, a $BaTiO_3$-based lead-free ceramic with outstanding piezoelectric properties

* Corresponding author.
E-mail address: xtan@iastate.edu (X. Tan).

https://doi.org/10.1016/j.jeurceramsoc.2018.03.049
Received 5 February 2018; Received in revised form 27 March 2018; Accepted 28 March 2018
Available online 30 March 2018
0955-2219/

[19–22]. *In-situ* TEM is employed to directly visualize the microstructure evolution corresponding to the macroscopic fatigue and aging degradation.

2. Materials and methods

2.1. Ceramics processing

The BZT–BCT polycrystalline ceramic was prepared through the solid-state reaction method. Stoichiometric amount of powders of $BaCO_3$ (99.8%), $CaCO_3$ (99.5%), ZrO_2 (99.5%), and TiO_2 (99.6%) were mixed and milled for 5 h in a planetary mill using ethanol and ZrO_2 milling media. The slurry was then dried and the powders were calcined at 1300 °C for 2 h. The calcined powder was again milled, dried, and formed into disks by uniaxial pressing in a 10 mm diameter die, followed by cold isostatic pressing at 300 MPa. Sintering was carried out at 1500 °C for 2 h, with a heating rate of 5 °C/min.

2.2. Bulk measurement

The sintered pellets were ground to a thickness of about 0.7 mm and silver electrodes were painted and fired on at 400 °C. The bipolar fatigue tests on bulk samples were conducted at room temperature using a triangular waveform at a frequency of 10 Hz. After fatigued for 10^6 cycles at ± 3.5 kV/cm, the sample was kept in air at room temperature for aging. The *P-E* hysteresis loops were recorded during the fatigue as well as the aging tests using a standardized ferroelectric test system (Precision LC II, Radiant Technologies).

2.3. In-situ TEM observation

As-sintered ceramic pellets were mechanically ground and polished down to 120 μm thick, and then ultrasonically cut into disks with a diameter of 3 mm. After dimpling and polishing, the disks were annealed at 150 °C for 2 h and Ar-ion milled until perforation. The *in-situ* TEM fatigue test was performed on an FEI Tecnai G2-F20 microscope operated at 200 kV, with bipolar electric fields in a triangle waveform at a frequency of 10 Hz applied to the specimen. The same TEM specimen, after subjected to 10^5 bipolar cycles at ± 60 V, was aged in air at room temperature. The specimen was then loaded to the TEM at a series of aging time to have its domain morphology examined and recorded.

In this work, we quote the applied voltage instead of the nominal electric field (applied voltage divided by the electrode spacing of 120 μm) because the TEM specimen contains many pores which either intensify or dilute the actual field and make the calculated nominal field misleading [23]. However, the magnitude of applied voltage was not arbitrarily chosen [24]. The voltage that can induce the single-domain state in the grain-of-interest is 108 V (Fig. 4a), while the electric field for the single-domain state in bulk samples is roughly 6 kV/cm [25]. To be consistent with the cycling condition (± 3.5 kV/cm) in bulk measurement, ± 60 V is used as the cyclic voltage for the *in-situ* TEM experiment.

3. Results

3.1. Macroscopic behavior of fatigue and aging

The *P-E* hysteresis loops measured before fatigue, after fatigue, and after aging are displayed in Fig. 1a. The switchable polarization ($2P_r$) hardly changes during fatigue but exhibits apparent degradation during aging (Fig. 1b). $2P_r$ decreases monotonically with the aging time, following the empirical logarithmic dependence [26]. In addition to the property decay, an obvious bump can be seen in the lower branch ($E > 0$) of the *P-E* loop in the aged state (Fig. 1a). The red dashed curve is created through the central inversion of the upper branch of the loop, in order to highlight this bump. The development of this bump shifts

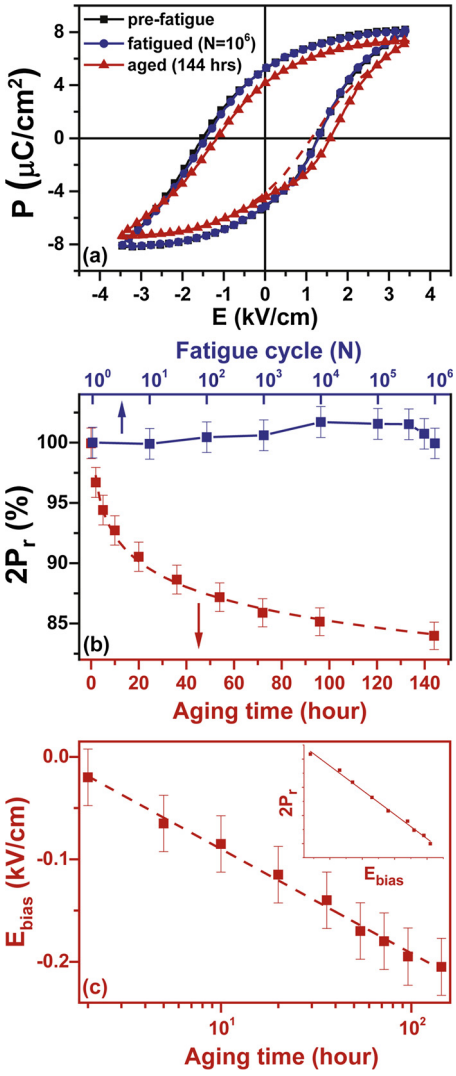

Fig. 1. (a) The*P-E* loops measured prior to fatigue, after fatigue, and after aging from the same sample. (b) The switchable polarization ($2P_r$) as a function of cycle number during fatigue and as a function of time during aging. (c) The development of the internal bias field (E_{bias}) during aging. The linear relation between E_{bias} and $2P_r$ displayed in the inset indicates a positive correlation between them. (For interpretation of the references to colour in the text, the reader is referred to the web version of this article.)

the *P-E* loop to the right, gradually building an internal bias field (E_{bias}), as depicted in Fig. 1c. It needs to be clarified that the observed shape change in the *P-E* loop is different from the "pinching" commonly seen in aged unpoled samples. They may even have different mechanisms, considering the following facts. First, defect dipoles must be rare in BZT–BCT due to absence of aliovalent dopants; second, there is no anomaly present in the *P-E* loop measured in the same sample which has been annealed and then aged for the same time period (144 h). The rightward shift of the *P-E* loop (Fig. 1a) and E_{bias} with negative values (Fig. 1c) imply that the aging process after electric cycling resembles that of a negatively poled sample [27]. This is reasonable because the last bipolar cycle stops when the negative voltage returns to zero. The voltage the sample sees last is with a negative polarity. Similar aging-induced changes in the shape of *P-E* loops have been previously reported in other "poled" $BaTiO_3$-based ceramics [28,29], where "poling" was completed simply by application of one cycle of unipolar fields rather than a dc voltage for an extended time.

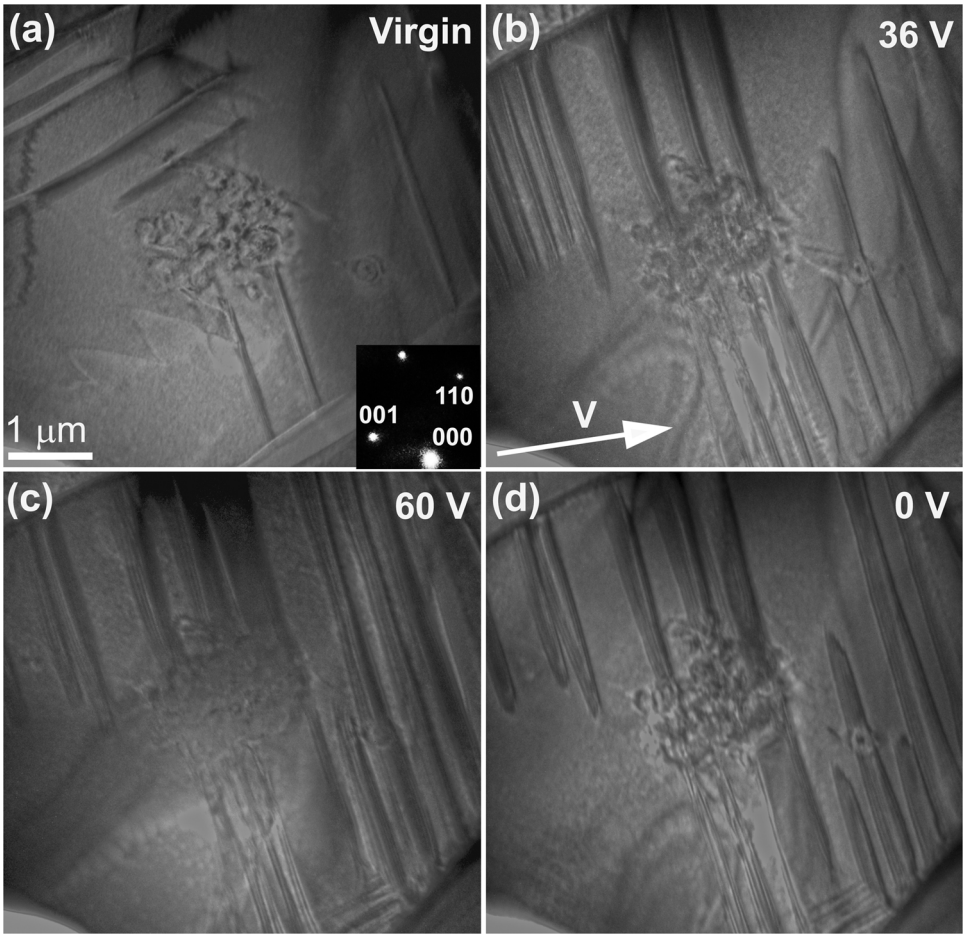

Fig. 2. *In-situ* TEM observations on the domain morphology evolution in a grain along its [$\bar{1}$10] zone-axis during the initial poling. Bright field micrographs recorded (a) in the virgin state, (b) at 36 V, (c) at 60 V and (d) after the applied voltage is removed. The inset in (a) is the electron diffraction pattern recorded at the virgin state. The long bright arrow in (b) indicates the positive direction of the applied voltage.

3.2. In-situ TEM observation of fatigue and aging

In order to uncover the microstructural origin of the macroscopic aging behavior, a grain along its [$\bar{1}$10] zone-axis is selected for the *in-situ* TEM observation (Fig. 2). In our previous *in-situ* TEM studies, the crystal symmetry is inferred primarily from the superlattice diffraction spots [30,31]. However, the various phases in BZT–BCT (*P4mm*, *R3m*, *Amm2*, *Pm*$\bar{3}$*m*) do not have superlattice spots in their electron diffraction patterns. Therefore, the diffraction patterns here are only used to assist the determination of the crystallographic information of the domain walls (inset of Fig. 2a). In the virgin state, a few long lamellar domains with domain walls tracing along < 111 > directions are embedded in the matrix (can be considered as a large domain, Fig. 2a). Crystallographic analysis indicates that the domain walls are very likely on {110} planes, suggesting the 71° rhombohedral domain walls. In addition to the lamellar domains, a feature of ~2 μm in size with an irregular shape and complex strain contrasts exists in the center of the observed area. The nature of this feature will be discussed in detail later. At the poling voltage of 36 V, some of the original domain walls which trace along the [11$\bar{1}$] direction are replaced by new domain walls tracing along the [111] direction, indicating the applied field is above the coercive field and domain switching starts to occur (Fig. 2b). Upon further increase of the poling voltage to 60 V, further changes in the domain configuration is noticed (Fig. 2c). After the voltage is removed, the domain morphology developed at 60 V is largely preserved (Fig. 2d).

The same area shown in Fig. 2 is monitored during the subsequent bipolar cycling with the peak voltage of 60 V and bright field micrographs are recorded after a certain number of cycles. It is noted that the applied voltage changes from –60 to 0 V at the end of bipolar cycling. During the first 10 cycles (Fig. 3a), a set of new domains are formed in the lower part of the observed area, which may be an indication of the domain instability in the initial stage of cycling [32]. However, domains in the rest part largely remain unchanged. Further application of bipolar fields to 10^5 cycles induces only minor changes in the domain configuration (Fig. 3b). Then, this specimen is kept on the TEM holder and is aged in air at room temperature. After 18 h aging (Fig. 3c), the overall domain morphology survives. But signs of aging start to emerge: several straight domain walls in the lower part of the observed area are partially disrupted by some complex features. After 42 h aging (Fig. 3d), the domain morphology changes significantly. A substantial number of lamellar domains have been disrupted to various degrees and are replaced by complex features. These complex features have identical appearances to the pre-existing large feature in the center of the observed area.

3.3. The nature of the features with complex contrast

Our previous *in-situ* TEM studies have reproducibly proved the existence of a unique single-domain state in the BZT–BCT ceramic at certain applied fields [8,33,34]. In this report, we take advantage of the transition towards the single-domain state to clarify the nature of those features with a complex contrast.

Voltages beyond 60 V are applied to the aged TEM specimen and the same area shown in Figs. 2 and 3 is focused. When the applied voltage reaches 108 V, all the long lamellar domains in the aged state (Fig. 3d)

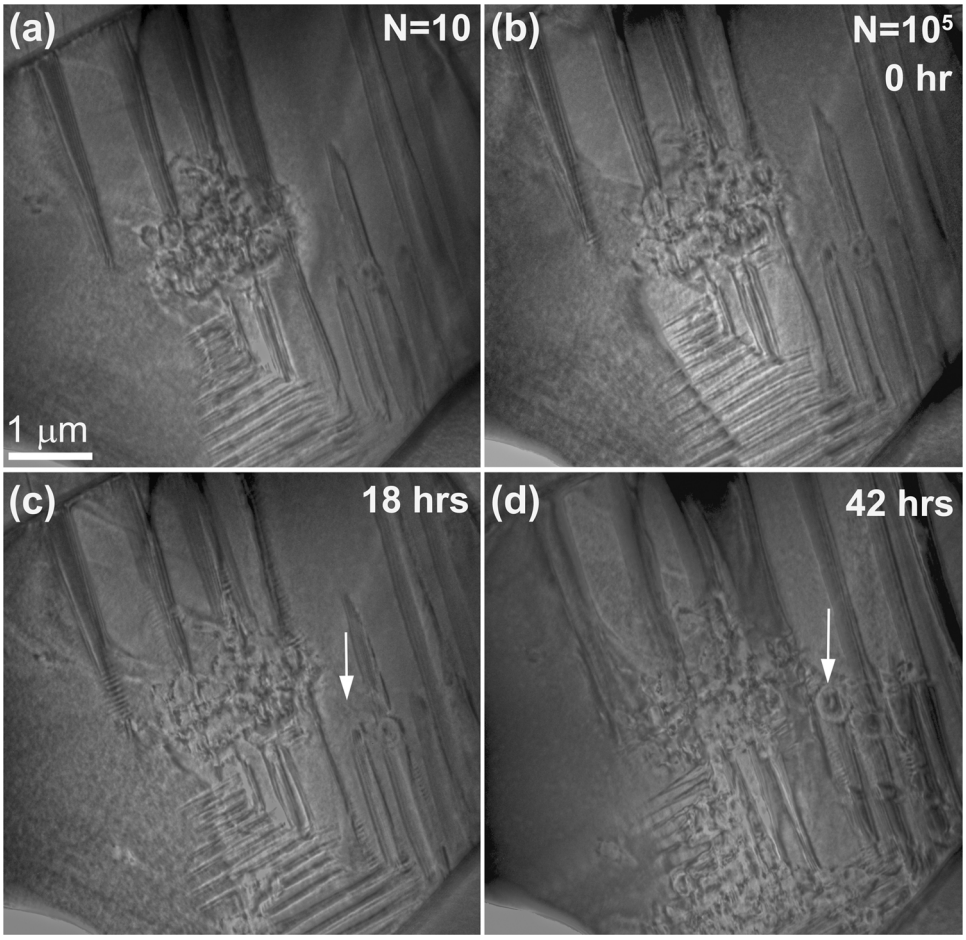

Fig. 3. Domain morphology evolution in the same area as in Fig. 2 during the electric cycling and the subsequent aging. Bright field micrographs recorded at 0 V after (a) 10, (b) 10^5 bipolar cycles of ± 60 V; and (c) 18, (d) 42 h in the subsequent aging. The aging process starts right after the 10^5 bipolar cycles fatigue test, denoted by "0 h" in (b). The bright arrows in (c) and (d) indicate the formation of a new defect cluster at the domain tip.

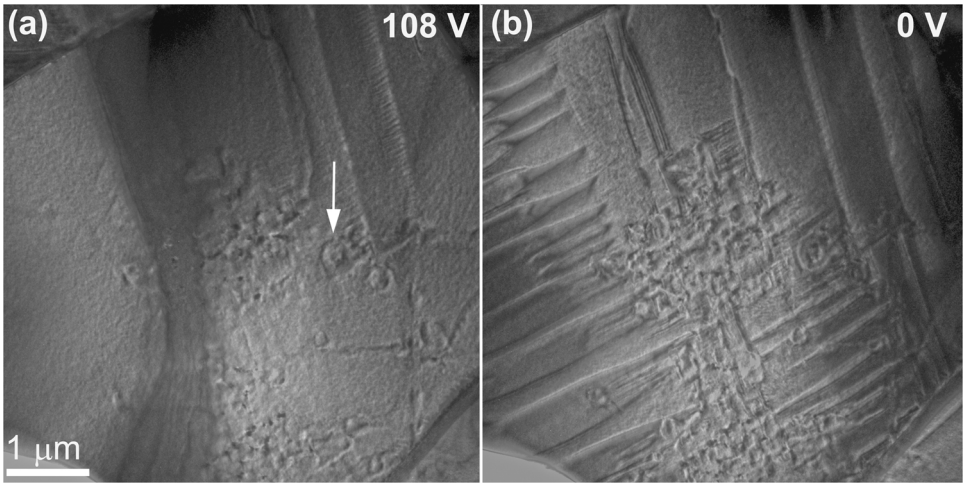

Fig. 4. Clarification of the nature of the features with a complex contrast. Bright field micrographs of the same area shown in Fig. 3(d) recorded (a) at 108 V and (b) after the voltage is removed. The bright arrow marks the same defect cluster in Fig. 3(d).

disappear completely (Fig. 4a), indicating a possible phase transition from the rhombohedral (*R3m*) to the orthorhombic phase (*Amm2*) [35]. It is worth noting that those complex features, both the pre-existing and the newly formed during aging, display obvious changes as well. The formerly complex contrasts become much cleaner while only some dark spots retain. Removal of the 108 V leads to the reappearance of large lamellar domains, but with a totally different configuration (Fig. 4b). Interestingly, the complex contrast of those features are recovered. Therefore, it can be deduced that those complex features are the mixture of clusters of charged point defects (most likely oxygen vacancies in BZT–BCT) and small fragmented domains. The oxygen vacancy clusters will not change under a single triangular field cycle, hence appear as the dark spots in Fig. 4a. On the other hand, the small fragmented domains can align their polarizations to merge with the matrix

large domain at 108 V and reappear at the removal of the applied voltage.

4. Discussion

The *in-situ* TEM observations on the domain structure evolution correlate well with the macroscopic behavior in the bulk measurement. The stable domain configuration against bipolar cycling at ± 60 V (Fig. 3a and b) is apparently the reason for the good fatigue resistance at ± 3.5 kV/cm in the bulk sample. Since the peak voltage for cycling (60 V) is way below the voltage needed to produce the single-domain state (108 V for the monitored grain, Fig. 4a), repeated domain switching rather than phase transition is expected to take place during bipolar cycling. In such a situation, domain fragmentation would be the most common consequence of electric fatigue [7,36]. However, the resilience of the long lamellar domains against fragmentation during cycling at ± 60 V can be attributed to the incomplete domain switching under the low applied fields. Baek et al. has shown in rhombohedral $BiFeO_3$ that fatigue degradation can only be rendered by complete 180° domain switching but not partial 71° domain switching [37]. So, ± 60 V, or ± 3.5 kV/cm, may not be sufficient to induce complete domain switching, thereby no obvious electric fatigue degradation is detected.

On the other hand, the apparent macroscopic aging in the bulk sample can be associated with the significant domain morphology change during the 42 h-aging in TEM. The development of the internal bias field during aging obeys the linear logarithmic time law, as shown by the fitted dashed line in Fig. 1c [17,38,39]. It has been widely hypothesized that, it is the depolarization field that drives the redistribution of oxygen vacancies and builds the E_{bias} [40,41]. Our *in-situ* TEM observations have provided strong support to this hypothesis. The domain morphology is quite stable against bipolar cycling but vulnerable to disruption with time in absence of applied fields. Similar phenomenon has been previously reported in ferroelectric thin films [42]. The depolarization field is reversed as the applied field changes polarity during cycling, which will redistribute the oxygen vacancies towards self-compensation. On the contrary, the depolarization field maintains its polarity during aging, hence forces a directional drift of oxygen vacancies and eventually builds the internal bias field. The disruption of lamellar domains with defect clusters during aging is a direct evidence that the depolarization field, instead of the applied field, is the driving force for oxygen vacancies' redistribution.

A close examination of the micrographs shown in Figs. 3 and 4 indicates that they further reveal the impact of domains on oxygen vacancy clustering. As pointed by the bright arrow in Fig. 3d, a circular-shaped feature with a diameter of ~0.4 μm forms at the tip of a domain after 42 h aging. For clarity, the same location is also marked in Fig. 3c where this feature has not formed yet. Also highlighted in Fig. 4a, this circular feature remains unchanged in shape and size under applied voltage of 108 V, indicating that it is a big cluster of oxygen vacancies. The high local electrostatic and elastic distortion energy at the domain tip accelerates the clustering process of oxygen vacancies. Clustered oxygen vacancies will in turn clamp the domain walls and suppress their responses to the applied fields [8]. In addition to being clamped at the tips, many lamellar domains are found to be disrupted and replaced by the mixture of oxygen vacancy clusters and fragmented domains after aging (Fig. 3d). This "domain disruption" during aging, even though appears in resemblance to the fatigue induced "domain fragmentation" [7], is resulted from completely different mechanisms. The clustering of oxygen vacancies at domain tips during aging is likely to be the first step. The accumulation of point defects at the tip then leads to the retraction of lamellar domains. As the aging process continues, domains will eventually be disrupted. This explains the observation in Fig. 3d that disruption primarily occurs to those relatively smaller lamellar domains having tips in the interior of the matrix large domain. The interactions of oxygen vacancy clusters at the tip with lamellar domains and the strong association of disrupted domains with point defects are apparently the micromechanisms for the degradation in switchable polarization ($2P_r$) during aging. Such a degradation in $2P_r$ is generally accompanied with the building up of E_{bias} [43]. The positive correlation is confirmed by the linear relation between $2P_r$ and E_{bias} shown in the inset of Fig. 1c.

5. Conclusions

The micromechanisms of aging in piezoelectric ceramics are investigated with *in-situ* TEM for the first time. Through contrasting the stability of domain morphology during fatigue and aging, depolarization field is proved to be the driving force for the redistribution of oxygen vacancies. During aging, oxygen vacancy clusters are directly observed to build up at the domain tips and then disrupt the lamellar domains into small fragments. As a result, the switchable polarization degrades apparently and an internal bias field builds up in the aged sample.

Acknowledgements

This work was supported by the National Science Foundation (NSF) through Grant DMR-1465254. TEM experiments were performed at the Sensitive Instrument Facility at Ames Laboratory, which is operated for the U.S. DOE by Iowa State University under Contract No. DE-AC02-07CH11358. The authors would like to thank Dr. Jurij Koruza for providing bulk ceramic samples.

References

[1] B. Jaffe, W.R. Cook, H. Jaffe, Piezoelectric Ceramics, Academic Press, London, 2012.
[2] J. Rödel, K.G. Webber, R. Dittmer, W. Jo, M. Kimura, D. Damjanovic, Transferring lead-free piezoelectric ceramics into application, J. Eur. Ceram. Soc. 35 (2015) 1659–1681.
[3] Y.A. Genenko, J. Glaum, M.J. Hoffman, K. Albe, Mechanisms of aging and fatigue in ferroelectrics, Mater. Sci. Eng. B 192 (2015) 52–82.
[4] V. Rojas, J. Koruza, E.A. Patterson, M. Acosta, X. Jiang, N. Liu, C. Dietz, J. Rödel, Influence of composition on the unipolar electric fatigue of $Ba(Zr0.2Ti_{0.8})O_3$-$(Ba_{0.7}Ca_{0.3})TiO_3$ lead-free piezoceramics, J. Am. Ceram. Soc. 100 (2017) 4699.
[5] S. Tsurekawa, H. Hatao, H. Takahashi, Y. Morizono, Changes in ferroelectric domain structure with electric fatigue in $Li_{0.06}(Na0.5K0.5)_{0.94}NbO_3$ ceramics, Jpn. J. Appl. Phys. 50 (2011) 09NC.
[6] V.V. Shvartsman, A.L. Kholkin, Fatigue-induced evolution of domain structure in ferroelectric lead zirconate titanate ceramics investigated by piezoresponse force microscopy, J. Appl. Phys. 98 (2005) 094109.
[7] H. Guo, X. Liu, J. Rödel, X. Tan, Nanofragmentation of ferroelectric domains during polarization fatigue, Adv. Funct. Mater. 25 (2015) 270–277.
[8] Z. Fan, C. Zhou, X. Ren, X. Tan, Domain disruption and defect accumulation during unipolar electric fatigue in a BZT–BCT ceramic, Appl. Phys. Lett. 111 (2017) 252902.
[9] X. Tan, J.K. Shang, Intersection of a domains in the c-domain matrix driven by electric field in tetragonal ferroelectric crystal, J. Appl. Phys. 95 (2004) 2805.
[10] X. Ren, Large electric-field-induced strain in ferroelectric crystals by point-defect-mediated reversible domain switching, Nat. Mater. 3 (2004) 91–94.
[11] L.X. Zhang, X. Ren, In situ observation of reversible domain switching in aged Mn-doped $BaTiO_3$ single crystals, Phys. Rev. B 71 (2005) 174108.
[12] L. Zhou, G. Rixecker, A. Zimmermann, F. Aldinger, Electric fatigue in antiferroelectric $Pb0.97La_{0.02}(Zr_{0.55}Sn_{0.33}Ti_{0.12})O_3$ ceramics induced by bipolar cycling, J. Eur. Ceram. Soc. 26 (2006) 883–889.
[13] C.C. Chou, C.S. Hou, T.H. Yeh, Domain pinning behavior of ferroelectric $Pb_{1-x}Sr_xTiO_3$ ceramics, J. Eur. Ceram. Soc. 25 (2005) 2505–2508.
[14] V.S. Postnikov, V.S. Pavlov, S.K. Turkov, Internal friction in ferroelectrics due to interaction of domain boundaries and point defects, J. Phys. Chem. Solids 31 (1970) 1785–1791.
[15] K. Carl, K.H. Hardtl, Electrical after-effects in Pb (Ti, Zr) O3 ceramics, Ferroelectrics 17 (1977) 473–486.
[16] M. Takahashi, Space charge effect in lead zirconate titanate ceramics caused by the addition of impurities, Jpn. J. Appl. Phys. 9 (1970) 1236.
[17] R. Lohkämper, H. Neumann, G. Arlt, Internal bias in acceptor-doped $BaTiO_3$ ceramics: numerical evaluation of increase and decrease, J. Appl. Phys. 68 (1990) 4220–4224.
[18] Y.A. Genenko, Aging of poled ferroelectric ceramics due to relaxation of random depolarization fields by space-charge accumulation near grain boundaries, Phys. Rev. B 80 (2009) 224109.
[19] M. Acosta, N. Novak, V. Rojas, S. Patel, R. Vaish, J. Koruza, G.A. Rossetti, J. Rödel, BaTiO3-based piezoelectrics: fundamentals, current status, and perspectives, Appl. Phys. Rev. 4 (2017) 041305.

[20] J.P. Praveen, T. Karthik, A.R. James, E. Chandrakala, S. Asthana, D. Das, Effect of poling process on piezoelectric properties of sol–gel derived BZT–BCT ceramics, J. Eur. Ceram. Soc. 35 (2015) 1785–1798.
[21] Y. Zhang, J. Glaum, M.C. Ehmke, K.J. Bowman, J.E. Blendell, M.J. Hoffman, The ageing and de-ageing behaviour of (Ba0. $85Ca_{0.15}$)($Ti_{0.9}Zr_{0.1}$)O_3 lead-free piezoelectric ceramics, J. Appl. Phys. 118 (2015) 124108.
[22] S. Su, R. Zuo, S. Lu, Z. Xu, X. Wang, L. Li, Poling dependence and stability of piezoelectric properties of Ba ($Zr0.2Ti_{0.8}$)O_3-(Ba $_{0.7}Ca_{0.3}$)TiO_3 ceramics with huge piezoelectric coefficients, Curr. Appl. Phys. 11 (2011) S120–S123.
[23] X. Tan, H. He, J.K. Shang, In situ transmission electron microscopy studies of electric-field-induced phenomena in ferroelectrics, J. Mater. Res.20 (2005) 1641–1653.
[24] Z.M. Fan, J. Koruza, J. Rödel, X. Tan, An ideal amplitude window against electric fatigue in $BaTiO_3$-based lead-free piezoelectric materials, Acta Mater. (2018) accepted.
[25] H. Guo, B.K. Voas, S. Zhang, C. Zhou, X. Ren, S.P. Beckman, X. Tan, Polarization alignment, phase transition, and piezoelectricity development in polycrystalline $0.5Ba(Zr0.2Ti_{0.8})O_3 - 0.5(Ba_{0.7}Ca_{0.3})TiO_3$, Phys. Rev. B 90 (2014) 014103.
[26] D. Damjanovic, Ferroelectric, dielectric and piezoelectric properties of ferroelectric thin films and ceramics, Rep. Prog. Phys. 61 (1998) 1267.
[27] E. Sapper, R. Dittmer, D. Damjanovic, E. Erdem, D.J. Keeble, W. Jo, T. Granzow, J. Rödel, Aging in the relaxor and ferroelectric state of Fe-doped (1-x)($Bi_{1/2}Na_{1/2}$)TiO_3-x$BaTiO_3$ piezoelectric ceramics, J. Appl. Phys. 116 (2014) 104102.
[28] S.K. Upadhyay, V.R. Reddy, K. Sharma, A. Gome, A. Gupta, Study of aging & de-aging behaviour in un-doped polycrystalline ferroelectric $BaTiO_3$, Ferroelectrics 437 (2012) 171–180.
[29] D.A. Hall, M.M. Ben-Omran, P.J. Stevenson, Field and temperature dependence of dielectric properties in $BaTiO_3$-based piezoceramics, J. Phys. Condens. Matter 10 (1998) 461.
[30] Z. Fan, X. Liu, X. Tan, Large electrocaloric responses in [$Bi_{1/2}$($Na,K)_{1/2}$]TiO_3-based ceramics with giant electro-strains, J. Am. Ceram. Soc. 100 (2017) 2088–2097.
[31] X. Liu, H. Guo, X. Tan, Evolution of structure and electrical properties with lanthanum content in [($Bi_{1/2}Na_{1/2}$) $0.95Ba_{0.05}]_{1-x}La_xTiO_3$ ceramics, J. Eur. Ceram. Soc. 34 (2014) 2997–3006.
[32] J. Nuffer, D.C. Lupascu, J. Rödel, Damage evolution in ferroelectric PZT induced by bipolar electric cycling, Acta Mater. 48 (2000) 3783–3794.
[33] H. Guo, C. Zhou, X. Tan, Unique single-domain state in a polycrystalline ferroelectric ceramic, Phys. Rev. B 89 (2014) 100104.
[34] M. Zakhozheva, L.A. Schmitt, M. Acosta, H. Guo, W. Jo, R. Schierholz, H.J. Kleebe, X. Tan, Wide compositional range in situ electric field investigations on lead-free Ba ($Zr0.2Ti_{0.8}$)O3 − x($Ba_{0.7}Ca_{0.3}$)TiO_3 piezoceramic, Phys. Rev. Appl. 3 (2015) 064018.
[35] Y. Nahas, A. Akbarzadeh, S. Prokhorenko, S. Prosandeev, R. Walter, I. Kornev, J. Iniguez, L. Bellaiche, Microscopic origins of the large piezoelectricity of leadfree (Ba,Ca)(Zr,Ti)O_3, Nat. Commun. 8 (2017) 15944.
[36] H. Simons, J. Glaum, J.E. Daniels, A.J. Studer, A. Liess, J. Rödel, M. Hoffman, Domain fragmentation during cyclic fatigue in 94%($Bi_{1/2}Na_{1/2}$)TiO_3-6%$BaTiO_3$, J. Appl. Phys. 112 (2012) 044101.
[37] S.H. Baek, C.M. Folkman, J.W. Park, S. Lee, C.W. Bark, T. Tybell, C.B. Eom, The nature of polarization fatigue in $BiFeO_3$, Adv. Mater. 23 (2011) 1621.
[38] G. Arlt, H. Neumann, Internal bias in ferroelectric ceramics: origin and time dependence, Ferroelectrics 87 (1988) 109–120.
[39] D. Wang, M. Cao, S. Zhang, Piezoelectric ceramics in the PbSnO3–Pb($Mg_{1/3}Nb_{2/3}$)O_3–$PbTiO_3$ ternary system, J. Am. Ceram. Soc. 94 (2011) 3690–3693.
[40] Y.A. Genenko, Space-charge mechanism of aging in ferroelectrics: an analytically solvable two-dimensional model, Phys. Rev. B 78 (2008) 214103.
[41] Y.A. Genenko, D.C. Lupascu, Drift of charged defects in local fields as aging mechanism in ferroelectrics, Phys. Rev. B 75 (2007) 184107.
[42] S.Y. Chen, V.C. Lee, Aging behavior and recovery of polarization in $Sr_{0.8}Bi_{2.4}Ta_2O_9$ thin films, J. Appl. Phys. 87 (2000) 3050–3055.
[43] U. Robels, L.S. Störmann, G. Arlt, Domain wall trapping as a result of internal bias fields, Ferroelectrics 133 (1992) 223–228.